DOI: 10.1002/((please add manuscript number))
Article type: Communication

Anomalous Photovoltaic Effect in Centrosymmetric Ferroelastic $BiVO_4$

Xitao Liu, Faqiang Zhang, Peiqing Long, Teng Lu, Huarong Zeng, Yun Liu, Ray L Withers, Yongxiang Li, and Zhiguo Yi**

Dr. X.T. Liu, Ms. P. Q. Long, Prof. Z. G. Yi
CAS Key Laboratory of Optoelectronic Materials Chemistry and Physics
Fujian Institute of Research on the Structure of Matter
Chinese Academy of Sciences
Fuzhou 350002, China
E-mail: zhiguo@fjirsm.ac.cn
Dr. F.Q. Zhang, Prof. H. R. Zeng, Prof. Y. X. Li
CAS Key Laboratory of Inorganic Functional Materials and Devices
Shanghai Institute of Ceramics
Chinese Academy of Sciences
Shanghai 200050, China
E-mail: yxli@mail.sic.ac.cn
Ms. T. Lu, Prof. Y. Liu, Prof. R.L.Withers
Research School of Chemistry
The Australian National University
Canberra, ACT 2601, Australia.
Prof. Z. G. Yi
University of Chinese Academy of Sciences
Beijing 100049, China

Keywords: ferroelectric photovoltaic, anomalous photovoltaic effect, $BiVO_4$

Anomalous photovoltaic (APV) effect is an intriguing phenomenon and rarely observed in bulk materials that structurally have an inversion symmetry. Here we report the discovery of such an APV effect in a centrosymmetric vanadate, $BiVO_4$, where noticeable above-bandgap photovoltage and a steady-state photocurrent are observed in both ceramics and single crystals even when illuminated under visible light. Moreover, the photovoltaic voltage could

be reversed by the stress modulation and a sine function relationship between photovoltage and stress directional angle is derived. Microstructure and strain field analysis reveal localized asymmetries that caused by strain fluctuations in bulk centrosymmetric $BiVO_4$. On the basis of the experimental results, a flexoelectric coupling via a strain induced local polarization mechanism is suggested to account for the APV effect observed. This work not only allows new applications for $BiVO_4$ in optoelectronic devices but also deepens insights into the mechanisms underlying the APV effect.

The anomalous photovoltaic (APV) effect, the generation of a steady photocurrent and above-bandgap photovoltage in a single-phase compound, has been studied for over fifty years.[1-7] It is generally acknowledged that the breaking of inversion symmetry is essential for the existence of an APV effect, although the mechanism/s underlying such behaviour remain under active debate.[8-14] From the technological point of view, a large and above-bandgap photovoltage is an attractive possibility with regards to new applications.[7, 15] The number of excellent materials that exhibit this intriguing effect, however, is very limited, especially when illuminated under visible light.[3-5]

Running parallel to research into the APV effect, $BiVO_4$ has also been studied for over fifty years.[16-20] It occurs naturally as the mineral pucherite with an orthorhombic structure type. Then, in 1963, Roth and Waring firstly synthesized $BiVO_4$ with a scheelite structure type.[16] Until 1975, Bierlein and Sleight discovered ferroelasticity in $BiVO_4$.[17] In the 1970's

$BiVO_4$ was also patented as a yellow pigment.[18] Hoffart *et al.* reported the ionic conductivity of $BiVO_4$ in 1996.[19] In 1999, the discovery of photocatalytic water oxidation over $BiVO_4$ led to intensive research on this material.[20] Nevertheless, $BiVO_4$ has never before been considered as a candidate for the APV effect because of its centrosymmetry.

In this article, we report an APV effect in centrosymmetric $BiVO_4$, which leads to the generation of a steady-state photovoltage over 40 V, exceeding the bandgap (~2.43 eV) by almost twenty times. It is found that this APV effect is associated with flexoelectric coupling where the photovoltaic response can be significantly modulated at various stress orientations.

The $BiVO_4$ ceramics used for this study were prepared by spark plasma sintering (SPS). X-ray diffraction (XRD) analysis of a crushed powder sample gave an *I*-centred, monoclinic scheelite-type structure[21] with lattice parameters a = 5.184 Å, b =5.083 Å, c = 11.693 Å, and $\gamma = 90.38^o$ (**Figure 1**a). Scanning electron microscopy (SEM) cross-sectional image (see inset in Figure 1a) shows dense ceramics with grain sizes ~3-5 μm, transgranular fracture behavior and sharp domain boundaries. The UV-visible diffuse reflectance spectrum (Figure 1b) indicates that $BiVO_4$ is a direct band gap semiconductor (E_g = 2.43 eV) that can absorb light with a wavelength shorter than ~530 nm, in good agreement with a previous report.[20]

The photovoltaic characterization was conducted on polished $BiVO_4$ ceramic samples using various device configurations. **Figure 2** shows the observed photoelectric properties using the device configuration presented in Figure 2a (electrode area ~ 0.34×5.02 mm^2 and electrode separation distance ~6.24 mm). A monochromatic light with a wavelength of 400

nm and a power intensity of 200 mW/cm^2 was employed. Current–voltage (*I*–*V*) curves measured both in the dark and under light illumination exhibit notable APV behavior (Figure 2b). In the dark, the $BiVO_4$ ceramic behaves like an insulator with an *I*-*V* curve that obeys Ohm's law. When the light is turned on, a large open-circuit voltage (V_{oc}) of 41 V was induced and a short-circuit current $I_{sc} \approx 0.67$ nA obtained, which is a unique feature of APV response distinguishing from conventional photovoltaic effects.[2, 7, 13] The ceramic behaves like an electric power source to generate a steady-state photovoltage over 40 V and a photocurrent ~ 0.65 nA under light illumination (Figures 2c and 2d). In both cases, the photoresponse remains unchanged as a function of time suggesting that thermal effects on the photovoltaic properties are negligible. The observed photocurrent (see the inset in Figure 2d) shows a rapid and quite repeatable photoresponse, exactly following the light switching on/off cycles. This high sensitivity and excellent retention of the photoresponse suggest that $BiVO_4$ might well have direct application in photosensitive devices.

As is well known, the photovoltaic effect in *p*-*n* junction semiconductors and ferroelectrics are influenced both by the incident photon energies (*e.g.* only photons with energies larger than the bandgap can be absorbed at all) as well as the power intensity of the illuminating light.[22, 23] Figure 2e shows the wavelength dependence of both the photovoltage and photocurrent of the $BiVO_4$ ceramic (see also Figure S1 in the Supporting Information). Both the photovoltage and photocurrent decrease with increasing wavelength *i.e.* with decreasing photon energy, in agreement with the optical absorption edge of the $BiVO_4$

semiconductor. Note that there is no obvious photovoltage or photocurrent observable when the corresponding energy is lower than the bandgap (*i.e.* when λ > 530 nm). These results show that interband excitation by light is essential for the observed APV effect of the $BiVO_4$ semiconductor. The photovoltage and photocurrent of the $BiVO_4$ ceramic measured at a monochromatic wavelength of 400 nm (see Figure 2f and Figure S2 in the Supporting Information) indicate that both V_{oc} and I_{sc} are linearly proportional to the incident light intensity. Since the photovoltaic performance of semiconductor materials is closely related to the excitation, separation and recombination of photo-generated carriers, the more electrons and holes that are excited the more opportunities the electrons and holes to be recombined, typically leading to a non-linear behaviour. The linear relationship between V_{oc} (I_{sc}) and light intensity observed herein indicates that there must be an internal field operating in the case of the $BiVO_4$ ceramics driving the separation and transportation of photo-generated electrons and holes.

Replacing the monochromatic light source by simulated solar light or collecting the photoelectric response using single crystals had little effect on the observed large APV effect (see Figures S3 and S4 in the Supporting Information), indicating that the APV effect has little relationship to either the type of light source used or the existence of ceramic grain boundaries. Note here, the V_{oc} difference between a $BiVO_4$ ceramic and single crystal is mainly attributed to the difference of their conductivities.

Given that the photovoltaic properties of ferroelectrics are known to be very sensitive to ferroelectric domain configuration,[4, 24, 25] we also investigated the impact of ferroelastic domain walls on the photovoltaic response of the $BiVO_4$ crystals. It is found that the APV effect could be observed in the modes both perpendicular and parallel to the domain walls (see Figure S5 in the Supporting Information), indicating that the domain walls model[4, 24] cannot be used to account for the observed APV effect in $BiVO_4$.

Interestingly, we noted that the APV effect of $BiVO_4$ could be modulated remarkably by polishing treatment (**Figure 3**): (I) Randomly polishing the sample results in normal photoconductivity while polishing the sample along the direction perpendicular to the electrode either enhances or reverses the photovoltage (Figure 3a); (II) Under the same light illumination conditions the value of the observed photovoltage is directly proportional to the separation distance between the two electrodes (Figure 3b); (III) When measuring the directional dependence of the photovoltage on applied stress (Figure 3c), we unexpectedly obtained a sine function relationship between photovoltage and the directional angle of the electrode rotation (Figure 3d).

The observed above-bandgap photovoltage in $BiVO_4$ in conjunction with the light intensity dependent photocurrent (Figure 2f) and electrode spacing dependent photovoltage (Figure 3b) strongly resembles the APV effect in non-centrosymmetric compounds (also called bulk photovoltaic effect in many literatures).[10, 12, 14] According to Fridkin *et al*,[12] an imbalanced electron (or hole) transition in the *k*-space of a compound without a center of

symmetry gives rise to an asymmetric momentum distribution of photoexcited charge carriers, leading to the generation of a steady short-circuit photocurrent density (J_{sc}), which can be written as:

$$J_{sc} = G\alpha I \quad (1),$$

where G, α, and I are the Glass coefficient, the absorption coefficient and the light intensity, respectively. Under the open-circuit condition, J_{sc} generates a steady-state photovoltage, which can be calculated as:

$$V_{oc} = \frac{J_{sc}}{\sigma + \sigma_{ph}} L = \frac{G\alpha I}{\sigma + \sigma_{ph}} L \quad (2),$$

where σ, σ_{ph} and L are the dark conductivity, the photoconductivity and the distance between the two electrodes, respectively. According to Equation (1), the J_{sc} generated by the APV effect increases linearly with light intensity. In addition, from Equation (2), one can obtain that the photovoltage V_{oc} is proportional to both light intensity and the distance between two electrodes L, and is not limited by the bandgap. Our observed photocurrent I_{sc} and photovoltage V_{oc} in $BiVO_4$ both fulfill exactly the two equations. In consideration of the fact that an APV effect was observed only in materials with broken "bulk or local" inversion symmetry,[8-14, 26] our results strongly suggest an analogous "polar" feature in $BiVO_4$.

Both second harmonic generation (SHG) as well as piezoresponse force microscopy (PFM) measurements were employed to test for broken bulk inversion symmetry. However, neither was an SHG response detected from the $BiVO_4$ crystals (see Figure S6 in the

Supporting Information), nor any PFM response obtained from the crystal surfaces (see Figure S7 in the Supporting Information).

Given this lack of any evidence for broken bulk inversion symmetry, high resolution TEM was then employed to investigate whether or not there are localized asymmetries in bulk centrosymmetric $BiVO_4$. **Figure 4**a (see also Figure S8 in the Supporting Information) shows a representative configuration of ferroelastic domain-walls in the $BiVO_4$ ceramic, observed by tilting the sample to the [001] zone axis direction. Each grain is typically subdivided into several domains by two sets of quasi-perpendicular domain walls. The width of the domain-walls ranges from about 1 nm to 20 nm. Figure 4b is an SAED pattern taken across the blue box labeled region of the inset in Figure 4a. Two split diffraction patterns can be observed due to the different orientation states of the two domains. The value of γ is measured to be 90.51° while the angle between the a_I and b_{II} axes is 0.98°. Hence, consistent with the four-fold rotational symmetry of the parent $BiVO_4$ phase, the diffraction pattern collected in the Domain I region overlaps with that obtained from the Domain II region if rotated by 89.53° (90.51° - 0.98°) counterclockwise. Figure 4c displays a HRTEM image, corresponding to the region labelled by the blue box in Figure 4a. Only one kind of atomic column can be observed. HRTEM simulation shows it corresponds to the heavy Bi/V atoms (inset in Figure 4c). The two domains, however, appear very similar to the eye.

To characterize the local lattice deformations, the $(\bar{2}20)$ lattice fringes of Domain I (Figures 4c and 4d) were selected to conduct a detailed geometric phase analysis (GPA) of

the local lattice strains.[27, 28] Maps of the local strain fields (ε_{xx}, ε_{yy}, and ε_{xy}) and lattice rotations (ω_{xy}) relative to Domain I are shown sequentially in Figures 4e-4h. When the coordinates of these maps are transformed to allow the *y*-axis of the strain fields to be parallel to the *b*-axis of Domain I (Figure 4i), it can be seen that the two domain regions are easily distinguished in the maps (Figures 4e-4h). The measured average values of ε_{xx}, ε_{yy}, ε_{xy} and ω_{xy} in Domain II are 1.5±0.5%, -1.6±0.5%, -0.4±0.4% and 1.0±0.3°, respectively, in good agreement with theoretical values (1.9%, -1.9%, -0.2% and 0.98°) estimated from the XRD and SAED data. It is noteworthy that two distinct domain-wall types, sharp and non-sharp, are observed in this system (Figure 4h). The non-sharp domain wall is in good agreement with the gradually changed width of the domain walls, as shown in Figure 4a. The most obvious distinction between the sharp and non-sharp walls is that the boundaries of the ε_{xx}, ε_{yy} and ε_{xy} fields are not consistent with each other for the non-sharp walls. On the right hand side of Figure 4f , the ε_{yy} map starts changing first while nothing has yet happened to the ε_{xx} map, leading to a negative shear strain (ε_{xy}) in the non-sharp domain-wall region. Thus, a continuous rotation replaces a discrete change in the domain-wall region. Finally, a transition in the ε_{xx} map in line with that at the sharp domain-wall, is accompanied by the retracement of the ε_{xy} map on the left hand side. Note that the continuous deformation process is good for relieving the local stress around incompatible domain-walls where the strain concentrates (dashed boxes), which can only be observed near sharp domain walls.

In addition to the two apparent types of domain-wall, the ubiquitous strain fluctuations (Figures 4e-4h) within domains is definitely worthy of further investigation. In Figure 4j, a reference lattice was therefore built to directly reveal the local atomic displacements of the projected Bi and V atoms in the various strain fluctuation areas. It can thereby be seen that the deviation of actual atomic positions from their ideal reference points is not due to signal noise or individual behavior. Island-shape nano-scale regions can thereby be drawn directly by means of the displacement vectors (Figure 4j). In the region shown, note that the generation, development, degeneration and disappearance of the deviations are quite continuous. Consistent with the results shown in the strain field maps (Figures 4e-4h), the existence of local tension and compression states can be expected because the gradient of the deviation corresponds to the local stress state of the lattice.

The above TEM analysis indicates that there are indeed localized asymmetries that caused by strain fluctuations in $BiVO_4$ though the compound possesses averagely bulk centrosymmetry. Given that flexoelectricity is a universal effect for all insulators and that the coupling between polarization and strain gradients on the nanoscale has been shown to lead to intriguing emergent properties,[29-31] it is suggested that the APV effect observed herein is associated with flexoelectric coupling via a strain induced local polarization mechanism (**Figure 5**). As is well known, $BiVO_4$ is a ferroelastic material in which the strain state can be sensitively tuned by an applied stress.[17] The finite sample dimension as well as the existence of ferroelastic domains allows the stress to relax in $BiVO_4$, thereby generating strain

gradients at surfaces and interfaces and finally leading to local polarization,[32, 33] *i.e.* to the flexoelectric effect. When random polishing is applied to a $BiVO_4$ ceramic, the local polarization of each domain and each grain will distribute randomly and eventually cancel out on the average, leading to normal photoconductivity. When unidirectional polishing is applied, however, the local polarization will not cancel out when averaged and then the intriguing APV effect is observed. The experimental results presented confirm exactly the above analysis. In particular, the change in sign of the photovoltage can be taken as an evidence of stress induced polarization reversal.

In summary, we report a large strain-induced APV effect in a structurally centrosymmetric ferroelastic $BiVO_4$ material. This work not only calls for re-appraisal of the mechanism underlying ferroelectric photovoltaic effects but also sheds new light on our understanding of the superior photocatalytic properties of $BiVO_4$.

Experimental Section

Sample preparation: The $BiVO_4$ ceramics were prepared by the spark plasma sintering (SPS) method using high-purity raw chemicals of Bi_2O_3 (99.0%, SCRC) and V_2O_5 (99.0%, SCRC). The raw chemicals were weighed according to the stoichiometric ratio 1:1 and then ball-milled in ethanol using zirconia balls for 12 h. The slurry was dried and calcined at 600°C for 8 h. The calcined powders were re-milled for 12 h and calcined a second time at 700°C for 8 h. The calcined powders were carefully ground with a mortar and pestle and then sieved with 300 meshes. The sieved powders were loaded into a graphite die (φ30 mm×φ10 mm×10 mm)

and sintered at 790°C for 10 min under a uniaxial pressure of 30 MPa and at a heating rate of 100 °C min^{-1} in vacuum by applying a pulsed direct electric current through the die using an SPS apparatus (SPS-211LX, SPS Syntex Inc., Kawasaki, Japan). The resultant ceramics were then cut into slices and thermally annealed at 500 °C for 4 h in O_2 to remove excess carbon. Single crystals of $BiVO_4$ used in this study were grown by a flux technique using Bi_2O_3/V_2O_5 as flux.[34, 35]

Physical Characterization: The crystal structures were identified using MinFlex II XRD equipment (Cu K_α radiation, Rigaku Co., Tokyo, Japan). The ceramic microstructures were observed using both SEM and TEM. For TEM analysis, electron transparent samples were achieved by punching the ceramic into disks with a diameter of 3 mm. These disks were then ground, polished, dimpled, and subsequently Ar-ion milled at low energy (2.5 keV) and low incidence angle (4-7°) in a stage cooled with liquid nitrogen to avoid irradiation damage. TEM, SAED and HRTEM investigations were carried out on a Tecnai F20 microscope. Geometric phase analysis (GPA**)** was performed using the Digital Micrograph GPA plug-in on HRTEM images. The optical absorption spectra of the samples were recorded using the diffuse reflection method on a PerkinElmer Lambda 900 UV/VIS/NIR spectrometer that was equipped with an integrating sphere covered with $BaSO_4$ as the reference. The second-harmonic generation (SHG) measurements were performed as set out in a previous investigation.[36] Piezoresponse force microscopy (PFM) using the commercial atomic force microscope (SPA 400, Seiko, Japan) was used to image any polar domains of the optically

polished $BiVO_4$ crystals. In the PFM, a platinum/titanium-coated silicon cantilever with spring constants of 2 N/m and a resonance frequency of 70 kHz was used. All measurements were performed under ambient conditions.

Photo-electric properties measurements: Before the electrical measurement, the sample surfaces were carefully polished and then coated with gold or silver electrodes. The photoelectric properties were measured at room temperature in air atmosphere with a Keithley 6517B electrometer. A CEL-HXUV300 xenon lamp was used for white light illumination and the monochromatic lights were obtained by inserting cut-off filters in between the light path. The incident light intensity was measured with a CEL-NP2000 optical power meter. Current-voltage (I-V) sweeps were measured starting from negative bias voltage of -100.0 V, proceeding to positive bias to the maximum voltage of +100.0 V. The voltage sweep rate was 1.0 V/s, dwell times per point ranged from 1.0 to 5.0 s and each curve were collected for at least three times. The short-circuit current and open-circuit voltage were recorded for every one second.

Supporting Information

Supporting Information is available from the Wiley Online Library or from the author.

Acknowledgements

X. T. Liu and F. Q. Zhang contributed equally to this work. This work was financially supported by the National Key R&D Program of China (2016YFA0201103), the Natural Science Foundation of China (Grant Nos. 21577143, 51502289 and 51502325), the Natural Science Foundation of Fujian Province (Grant No. 2016J05144), and the Frontier Science

Key Project of the Chinese Academy of Sciences (QYZDB-SSW-JSC027). Y. Liu thanks the Australian Research Council for support in the form of an ARC discovery program grant.

Received: ((will be filled in by the editorial staff))
Revised: ((will be filled in by the editorial staff))
Published online: ((will be filled in by the editorial staff))

References

[1] M. E. Lines, A. M. Glass, *Principles and Applications of Ferroelectrics and Related Materials*, Clarendon Press, **1977**.

[2] V. M. Fridkin, *Photoferroelectrics*, Vol. 9, Springer Science & Business Media, **1979**.

[3] T. Choi, S. Lee, Y. J. Choi, V. Kiryukhin, S. W. Cheong, *Science* **2009**, 324, 63.

[4] S. Y. Yang, J. Seidel, S. J. Byrnes, P. Shafer, C. H. Yang, M. D. Rossell, P. Yu, Y. H. Chu, J. F. Scott, J. W. Ager III, L. W. Martin, R. Ramesh, *Nature Nanotech.* **2010**, 5, 143.

[5] R. Nechache, C. Harnagea, S. Li, L. Cardenas, W. Huang, J. Chakrabartty, F. Rosei, *Nature Photonics* **2015**, 9, 61.

[6] J. E. Spanier, V. M. Fridkin, A. M. Rappe, A. R. Akbashev, A. Polemi, Y. Qi, Z. Gu, S. M. Young, C. J. Hawley, D. Imbrenda, G. Xiao, A. L. Bennett-Jackson, C. L. Johnson, *Nature Photonics* **2016**, 10, 611.

[7] C. Paillard, X. Bai, I. C. Infante, M. Guennou, G. Geneste, M. Alexe, J. Kreisel, B. Dkhil, *Adv. Mater.* **2016**, 28, 5153.

[8] V. M. Fridkin, B. N. Popov, *Sov. Phys. Usp.* **1978**, 21, 981.

[9] R. V. Baltz, *Phys. Status Solidi B* **1978**, 89, 419.

[10] V. I. Belinicher, B. I. Sturman, *Sov. Phys. Usp.* **1980**, 23, 199.

[11] R.V. Baltz, W. Kraut, *Phys. Rev. B* **1981**, 23, 5590.

[12] V. M. Fridkin, *Crystallogr. Rep.* **2001**, 46, 654.

[13] P. Lopez-Varo, L. Bertoluzzi, J. Bisquert, M. Alexe, M. Coll, J. Huang, J. A. Jimenez-Tejada, T. Kirchartz, R. Nechache, F. Rosei, Y. Yuan, *Phys. Rep.* **2016**, 653, 1.

[14] L. Z. Tan, F. Zheng, S. M. Young, F. Wang, S. Liu, A.M. Rappe, *npj Comput. Mater.* **2016**, 2, 16026.

[15] J. Kreisel, M. Alexe, P. A. Thomas, *Nature Mater.* **2012**, 11, 260.

[16] R. S. Roth, J. L. Waring, *Am. Miner.* **1963**, 48, 1348.

[17] J. D. Bierlein, A. W. Sleight, *Solid State Commun.* **1975**, 16, 69.

[18] D. H. Piltingsrud, *US Patent*: 4115141, **1978**.

[19] T. Lu, B. C. H. Steele, *Solid State Ionics* **1986**, 21, 339.

[20] A. Kudo, K. Omori, H. Kato, *J. Am. Chem. Soc.* **1999**, 121, 11459.

[21] W. I. F. David, A. M. Glazer, A. W. Hewat, *Phase Transit.* **1979**, 1, 155.

[22] S. D. Stranks, H. J. Snaith, *Nature Nanotech.* **2015**, 10, 391.

[23] I. Grinberg, D. V. West, M. Torres, G. Gou, D. M. Stein, L. Wu, G. Chen, E. M. Gallo, A. R. Akbashev, P. K. Davies, J. E. Spanier, A. M. Rappe, *Nature* **2013**, 503, 509.

[24] J. Seidel, D. Fu, S.-Y. Yang, E. Alarcón-Lladó, J. Wu, R. Ramesh, J. W. Ager, *Phys. Rev. Lett.* **2011**, 107, 126805.

[25] A. Bhatnagar, A. R. Chaudhuri, Y. H. Kim, D. Hesse, M. Alexe, *Nature Commun.* **2013**, 4, 2835.

[26] F. G. Wang, S. M. Young, F. Zheng, I. Grinberg, A. M. Rappe, *Nature Commun.* **2016**, 7, 10419.

[27] J. L. Rouviere, E. Sarigiannidou, *Ultramicroscopy* **2005**, 106, 1.

[28] M. J. Hytch, *Microsc. Microanal. Microstruct.* **1997**, 8, 41.

[29] G. Catalan, A. Lubk, A.H.G. Vlooswijk, E. Snoeck, C. Magen, A. Janssens, G. Rispens, G. Rijnders, D. H.A. Blank, B. Noheda, *Nature Mater.* **2011**, 10, 963.

[30] P. Zubko, G. Catalan, A. K. Tagantsev, *Annu.Rev.Mater. Res.* **2013**, 43, 387.

[31] S.V. Kalinin, A. N. Morozovska, *Nature Nanotech.* **2015**, 10, 917.

[32] R. Munprom, P. A. Salvador, G. S. Rohrer, *Chem. Mater*. **2014**, 26, 2774.

[33] P. Zubko, G. Catalan, A. Buckley, P. R. L.Welche, J. F. Scott, *Phys. Rev. Lett.* **2007**, 99, 167601.

[34] D. Elwell, *Crystal growth from high-temperature solutions*, Scheel, Hans J, **2011**.

[35] D. S. Feng, X. T. Liu, J. Wang, Z. G. Yi, *J. Synth. Cryst.*(in Chinese) **2014**, 43, 3104.

[36] X. T. Liu, P. Q. Long, Z. H. Sun, Z. G. Yi, *J. Mater. Chem. C* **2016**, 4, 7563.

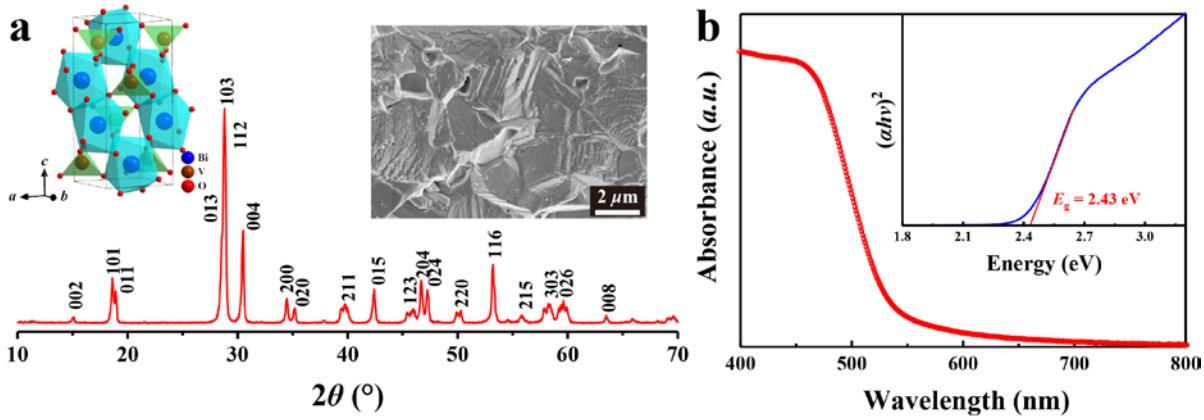

Figure 1. Physical characterization of $BiVO_4$. **a**, XRD pattern of $BiVO_4$ ceramic powders. Left inset: Schematic drawing of the crystal structure. Right inset: Cross-sectional SEM image of the prepared $BiVO_4$ ceramic. **b**, UV - visible diffuse reflectance spectrum of the $BiVO_4$ ceramic. Inset shows a plot of the calculation used to determine the band gap.

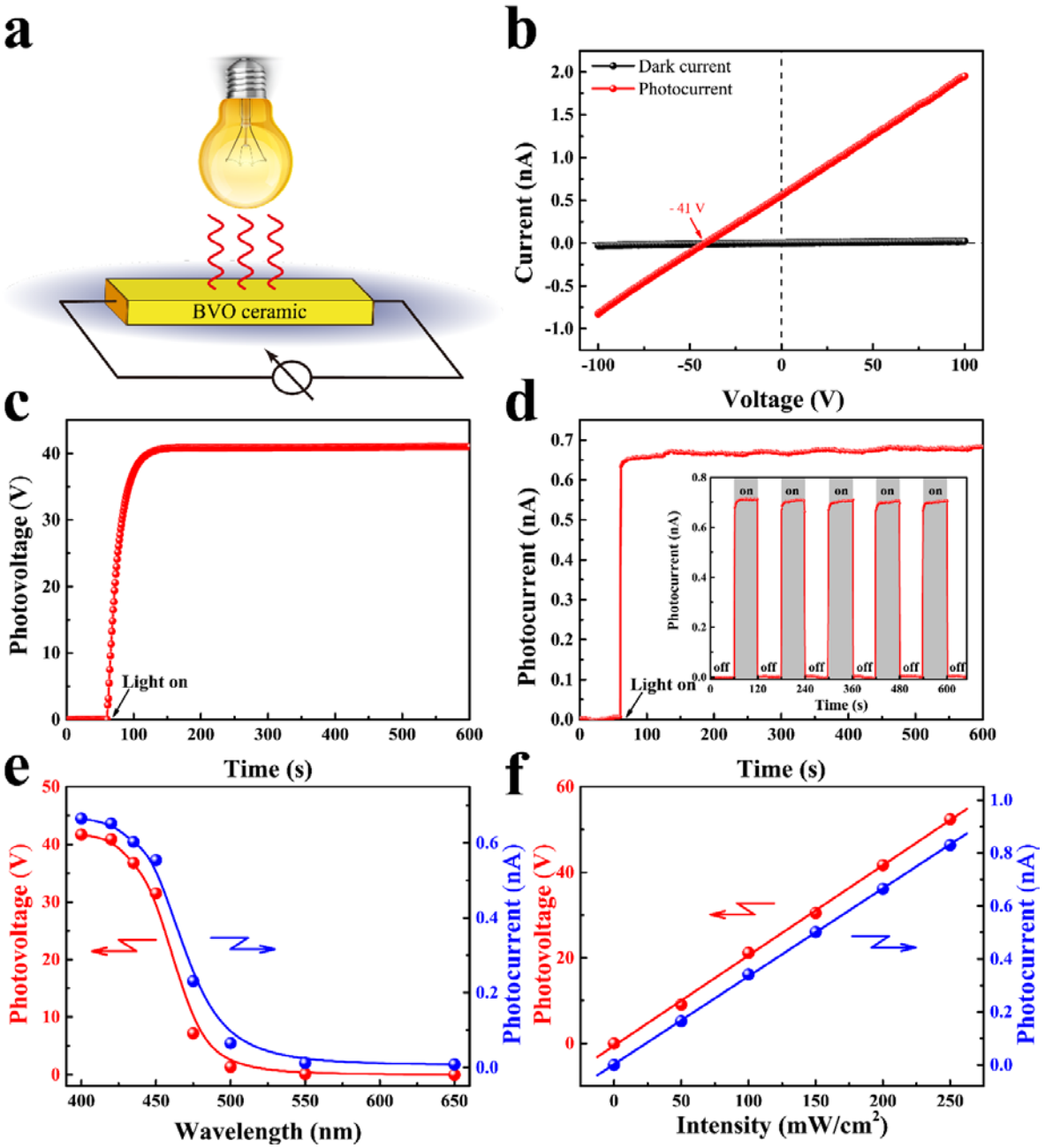

Figure 2. Photoelectric properties of $BiVO_4$ ceramics. **a**, Schematic diagram of the device configuration (0.34×5.02 mm^2 electrode area and 6.24 mm electrode spacing). **b**, *I-V* curves characterized under dark and 400 nm monochromatic light (200 mW/cm^2) illumination. **c**, Open-circuit voltage (V_{oc}) as a function of time when the light is turned on. **d**, Short-circuit current (I_{sc}) as a function of time when the light is turned on. Inset to **d**, the *I-t* response under repeated light on and off switching. **e**, Wavelength dependence of V_{oc} and I_{sc} at fixed light intensity of 200 mW/cm^2. **f**, Light intensity dependence of V_{oc} and I_{sc} under 400 nm monochromatic light illumination.

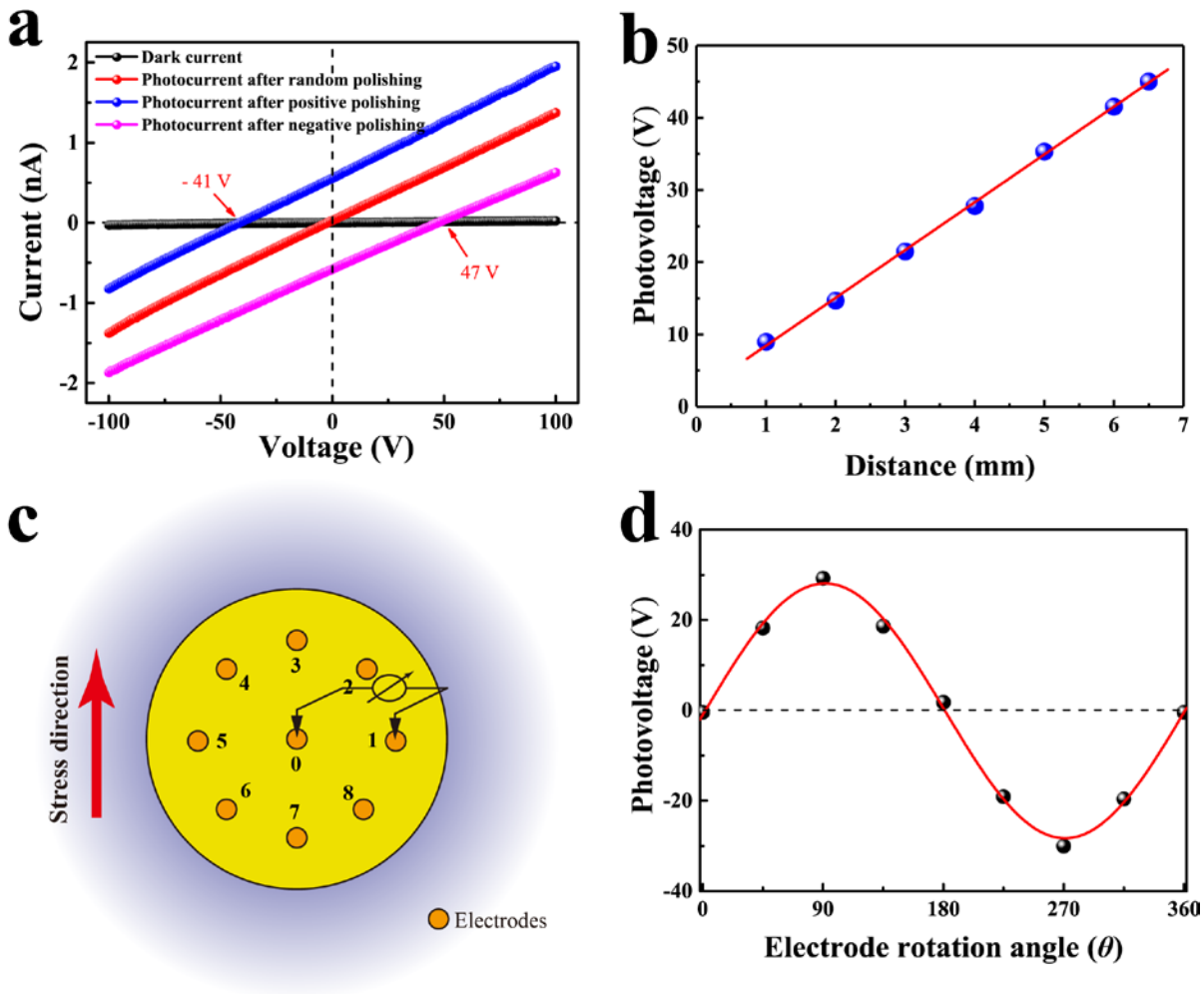

Figure 3. Role of stress on the photovoltaic response. **a**, *I-V* characteristics of $BiVO_4$ ceramics with different polishing treatments under dark and 400 nm monochromatic light (200 mW/cm^2) illumination. **b**, V_{oc} as a function of the distance between the electrodes. **c**, Schematic illustration of the electrode geometries (0.785 mm^2 circular electrode area and 5.0 mm electrode spacing) used for the photovoltaic measurements in **d**. **d**, Electrode rotation angle dependence of V_{oc} for a $BiVO_4$ ceramic treated with unidirectional polishing. The angle θ is counted anticlockwise from 0 (the 0⟶1 in **c**) to 360°.

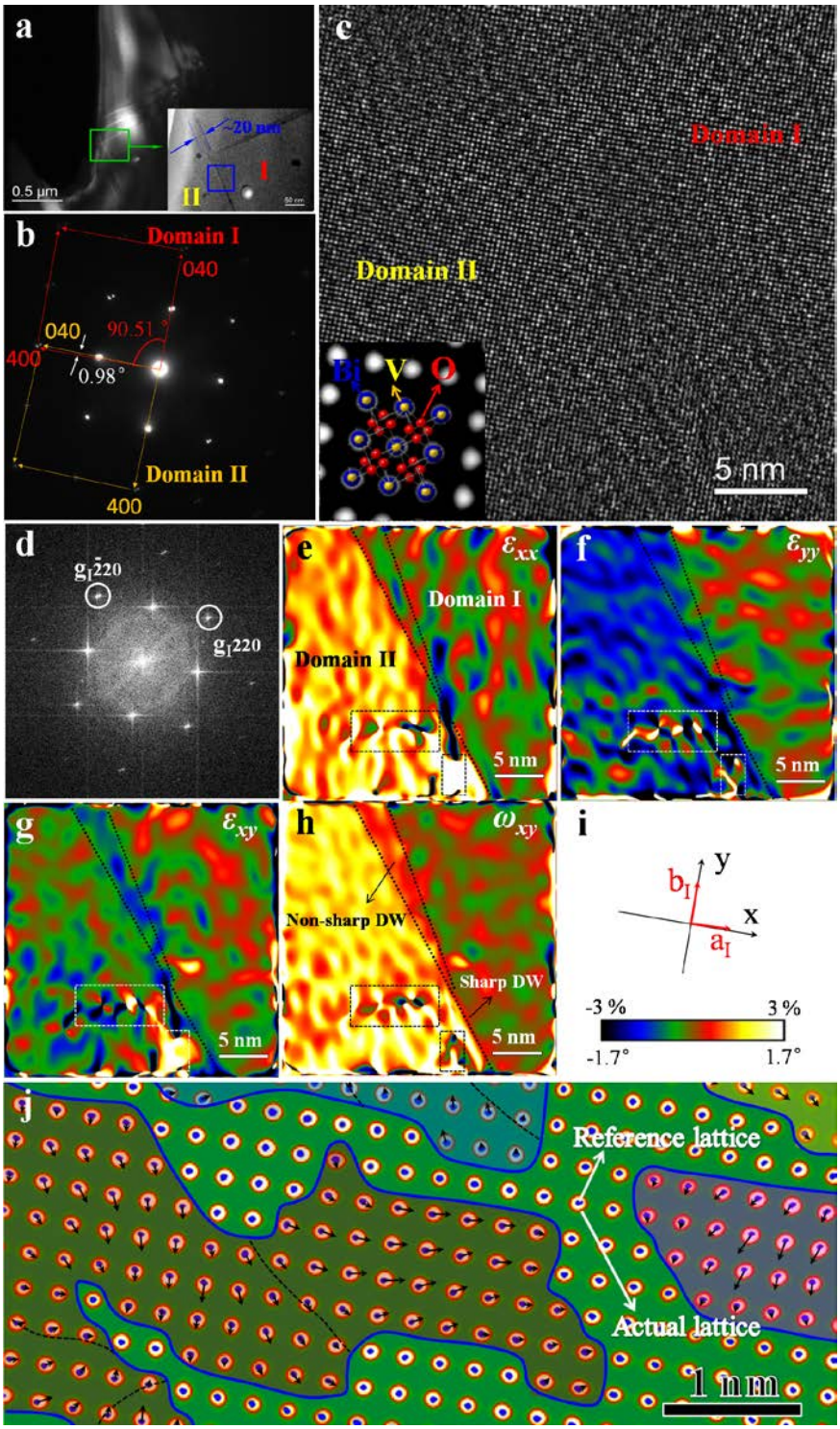

Figure 4. Microstructure characterization and strain field analysis. **a**, Configuration of domains in $BiVO_4$ grain. **b**, SAED pattern. **c**, HRTEM image of the local lattice along the [001] direction taken from the blue box marked region in image **a**. Inset shows the HRTEM simulation image. **d**, Fourier transform of image **c**. **e-h**, In-plane strain tensor components ε_{xx}, ε_{yy}, shear ε_{xy} and lattice rotation ω_{xy} deduced by geometric phase analysis (GPA). **i**, Coordinates relations and color scale of the strain field maps. The reference lattice for the GPA analysis was selected from domain I far from the domain-wall. **j**, Map of the atomic displacement vectors building on the FFT filtered HRTEM image in domain I. The reference lattice, i.e. nuclear-like points, was built by moving the actual lattice, after shrinkage, over a distance of one unit cell along the $(\bar{2}20)$ direction.

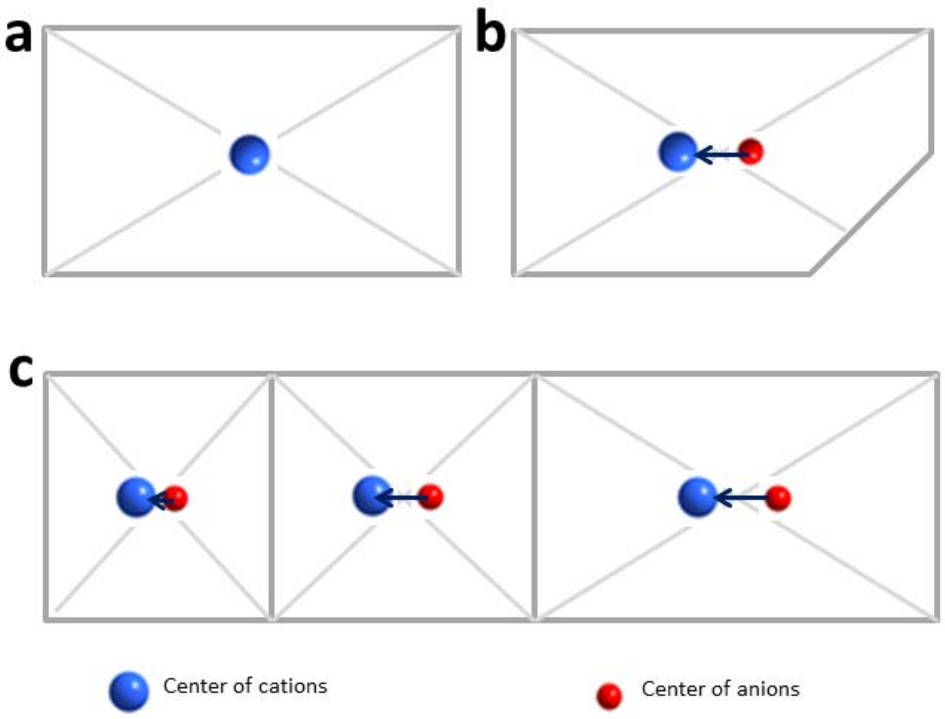

Figure 5. Schematic drawing illustrate the flexoelectric coupling via a strain induced local polarization mechanism in $BiVO_4$. **a**, Unstrained $BiVO_4$ has a centrosymmetry and the net dipole moment of the unit cell is zero. **b**, Non-uniform distortion, for example the lattices close to the domain boundaries, makes $BiVO_4$ lose centrosymmetry and thus induces a net dipole moment in the deformed unit cell. **c**, Unidirectional polishing results in non-uniform compression and stretching of the $BiVO_4$ lattices, which also produces net dipole moments.

The table of contents entry

Anomalous photovoltaic (APV) effect is discovered in a centrosymmetric vanadate, $BiVO_4$, where noticeable above-bandgap photovoltage and a steady-state photocurrent are observed in both ceramics and single crystals even when illuminated under visible light. Moreover, the photovoltaic voltage could be reversed by the stress modulation and a sine function relationship between photovoltage and stress directional angle is derived.

Keywords: ferroelectric photovoltaic, anomalous photovoltaic effect, $BiVO_4$

Xitao Liu, Faqiang Zhang, Peiqing Long, Teng Lu, Huarong Zeng, Yun Liu, Ray L Withers, Yongxiang Li*, and Zhiguo Yi*

Title: Anomalous Photovoltaic Effect in Centrosymmetric Ferroelastic $BiVO_4$

ToC figure

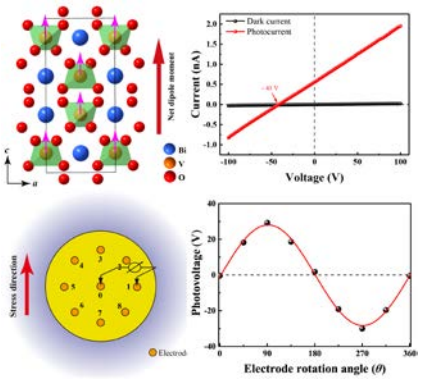

Supporting Information

Anomalous Photovoltaic Effect in Centrosymmetric Ferroelastic $BiVO_4$

Xitao Liu, Faqiang Zhang, Peiqing Long, Teng Lu, Huarong Zeng, Yun Liu, Ray L Withers, Yongxiang Li, and Zhiguo Yi**

Dr. X.T. Liu, Ms. P. Q. Long, Prof. Z. G. Yi
CAS Key Laboratory of Optoelectronic Materials Chemistry and Physics
Fujian Institute of Research on the Structure of Matter
Chinese Academy of Sciences
Fuzhou 350002, China
E-mail: zhiguo@fjirsm.ac.cn
Dr. F.Q. Zhang, Prof. H. R. Zeng, Prof. Y. X. Li
CAS Key Laboratory of Inorganic Functional Materials and Devices
Shanghai Institute of Ceramics
Chinese Academy of Sciences
Shanghai 200050, China
E-mail: yxli@mail.sic.ac.cn
Ms. T. Lu, Prof. Y. Liu, Prof. R.L.Withers
Research School of Chemistry
The Australian National University
Canberra, ACT 2601, Australia.
Prof. Z. G. Yi
University of Chinese Academy of Sciences
Beijing 100049, China

The Supplementary Info includes:

Figures S1-8

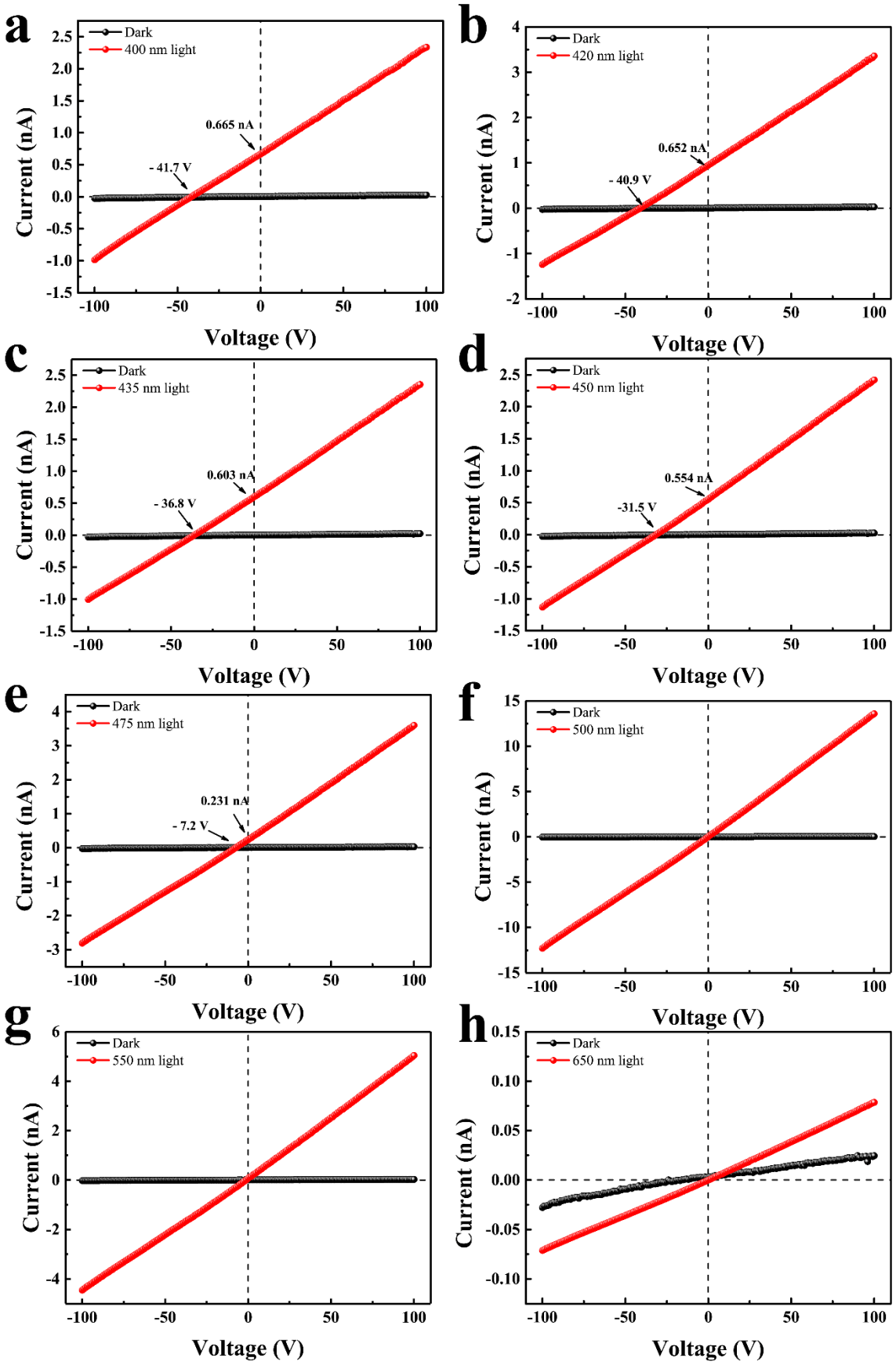

Figure S1. I-V curves of $BiVO_4$ ceramics collected under various monochromatic light illumination with light intensity of 200 mW/cm^2.

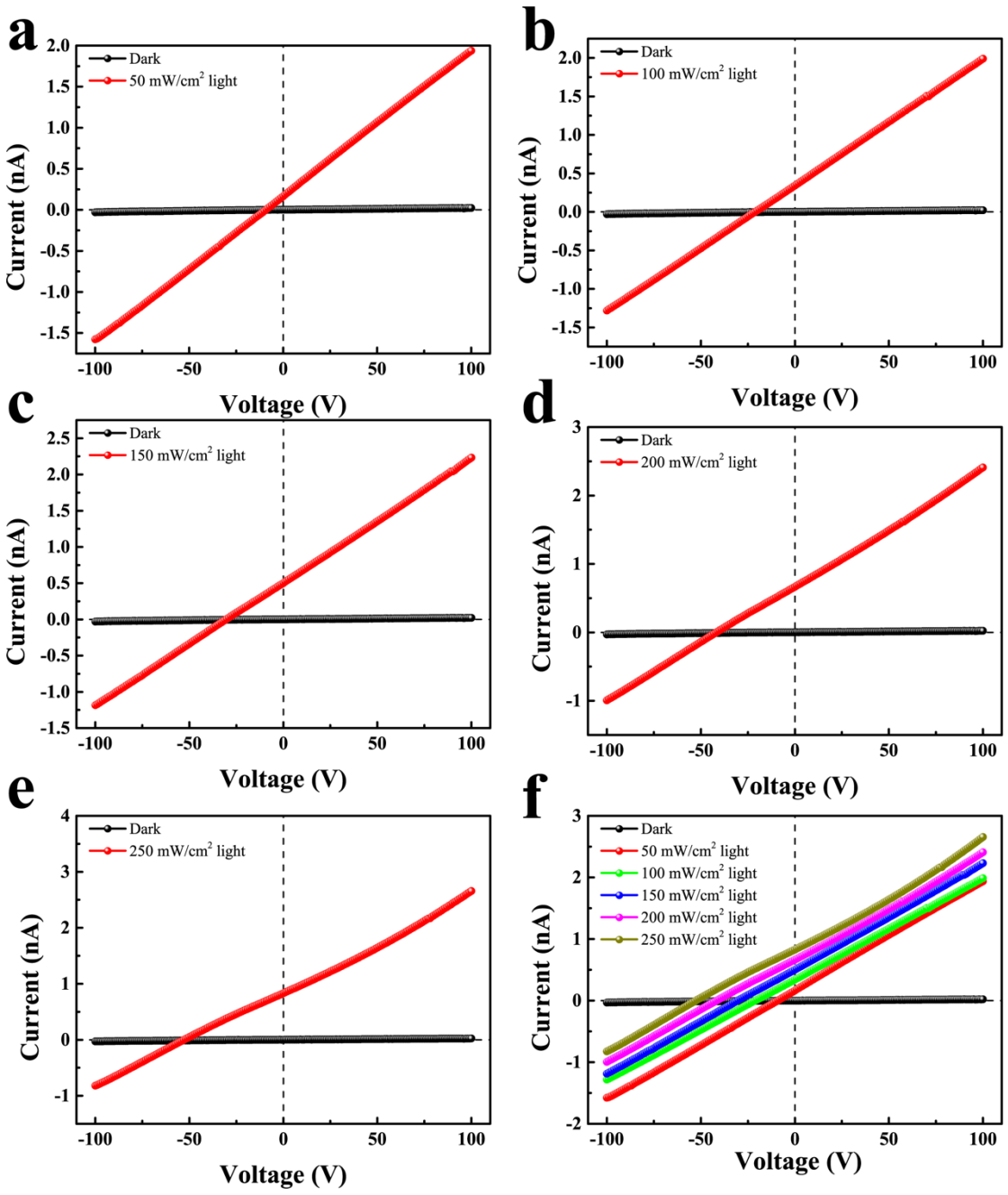

Figure S2. I-V curves of $BiVO_4$ ceramics collected under 400 nm monochromatic light illumination at different light intensities.

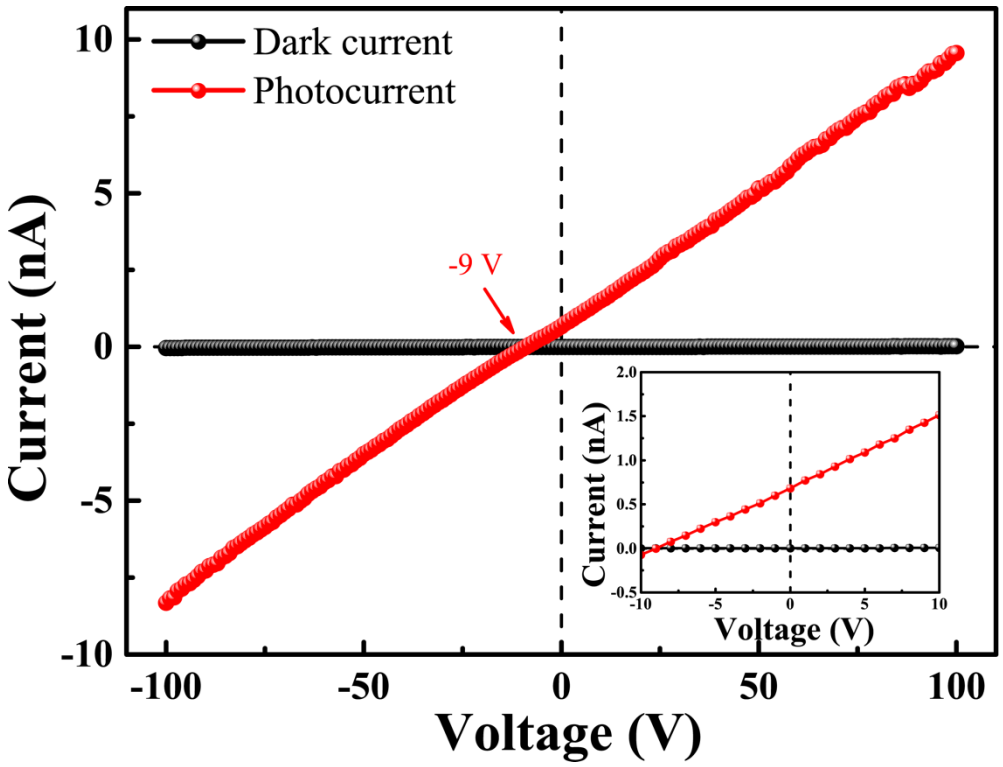

Figure S3. I-V curve of $BiVO_4$ ceramics under white light illumination (~200mW/cm^2).

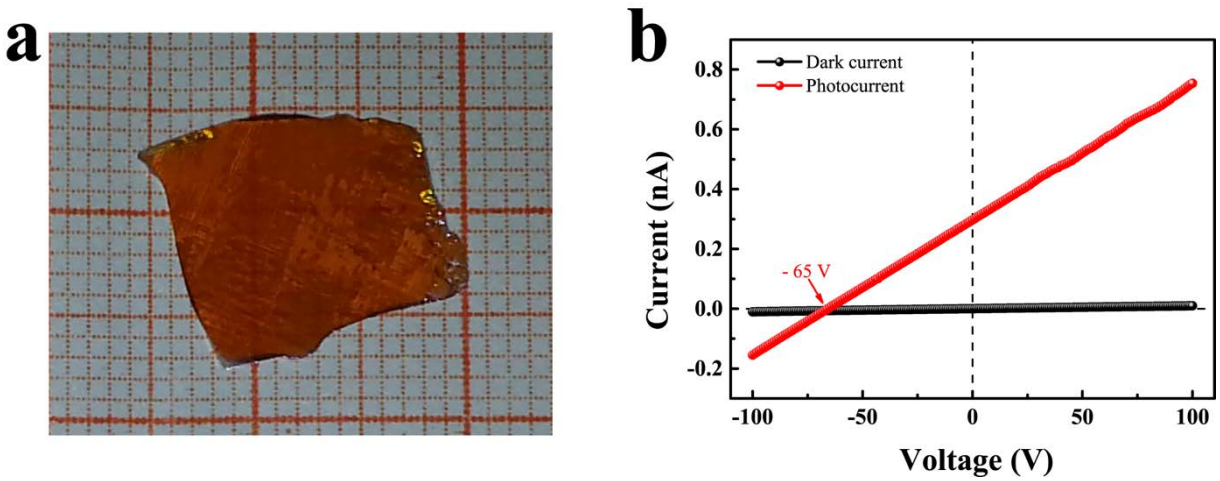

Figure S4. Anomalous photovoltaic effect in a $BiVO_4$ single crystal. **a**, Photograph of the as grown $BiVO_4$ single crystal. **b**, I-V curve of the $BiVO_4$ crystal with electrode area ~0.38×5.82 mm^2 and electrode separation distance ~7.24 mm under 400 nm monochromatic light illumination (~200 mW/cm^2).

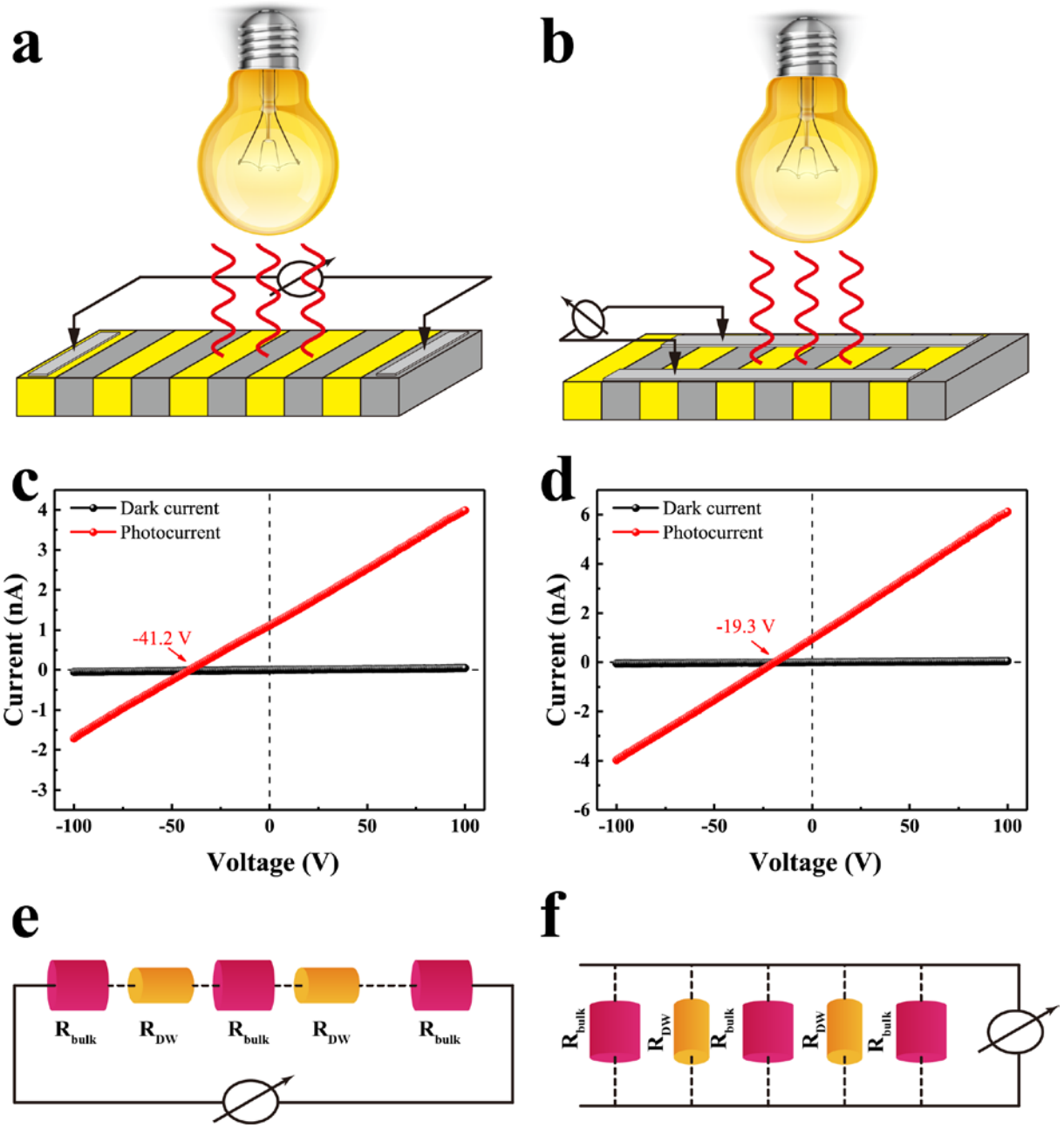

Figure S5. Role of domain walls on the photovoltage response. **a** and **b,** Schematics of the perpendicular ($DW_{\perp}$) (**a**) and parallel ($DW_{\parallel}$) (**b**) device configuration. **c** and **d,** Corresponding *I-V* measurements of the perpendicular and parallel devices, respectively. **e** and **f**, An equivalent circuit considering that the domain bulk and domain wall have different resistances, R_{bulk} and R_{DW}, is shown for both perpendicular and parallel devices.

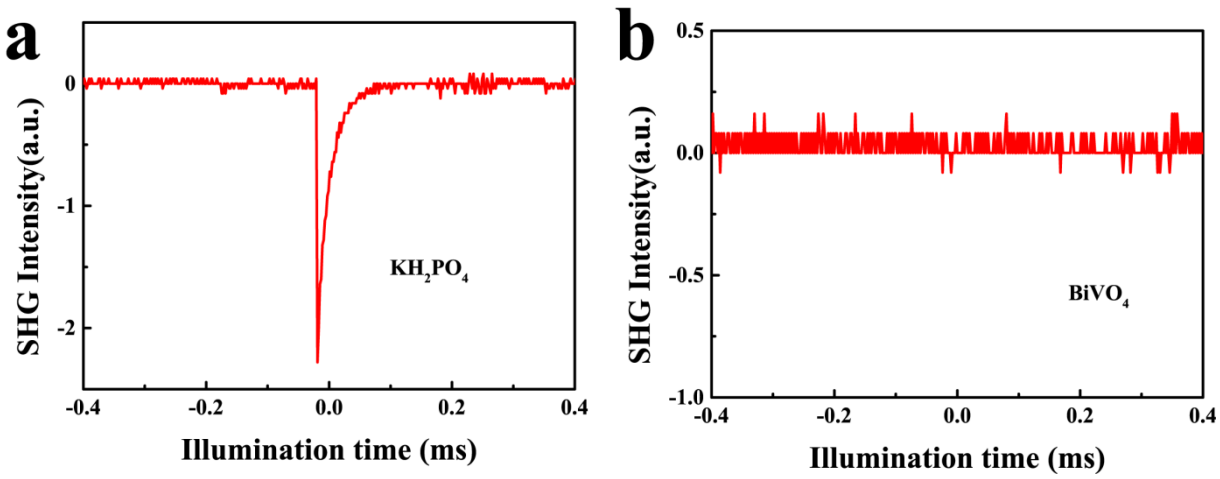

Figure S6. Results of second harmonic generation (SHG) measurements. **a**, SHG signals of KH_2PO_4 (KDP). **b**, Oscilloscope traces of SHG signals from $BiVO_4$.

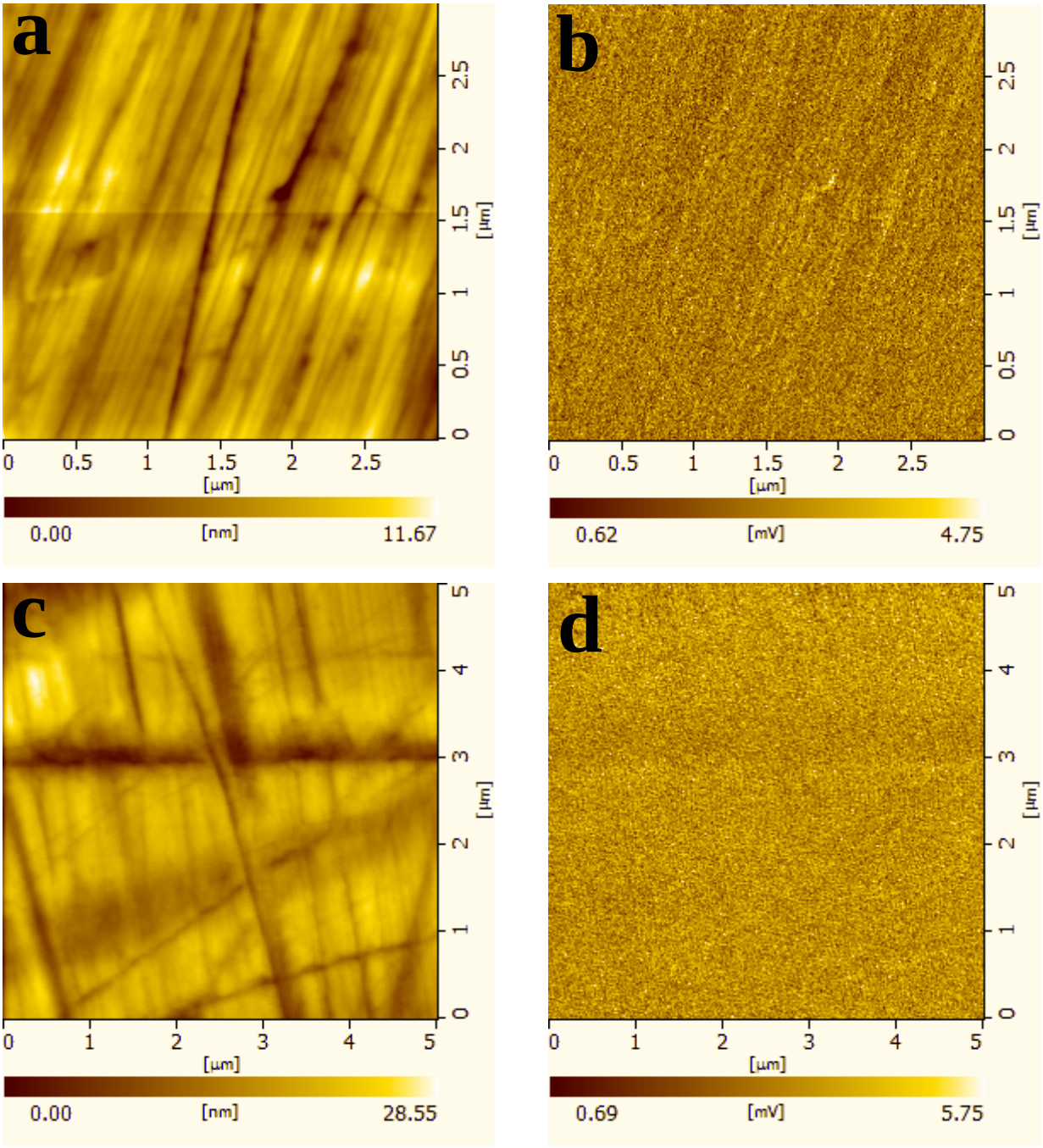
a
0
0.5
1
1.5
2
2.5
[µm]
0.00
[nm]
11.67
b
0.62
[mV]
4.75
c
0
1
2
3
4
5
0.00
[nm]
28.55
d
0.69
[mV]
5.75

Figure S7. Atomic Force Microscopy characterization of $BiVO_4$ crystals. **a** and **c**, AFM topographic images of (010) and (101) crystal planes, respectively. **b** and **d**, out-of-plane PFM images of (010) and (101) crystal planes, respectively.

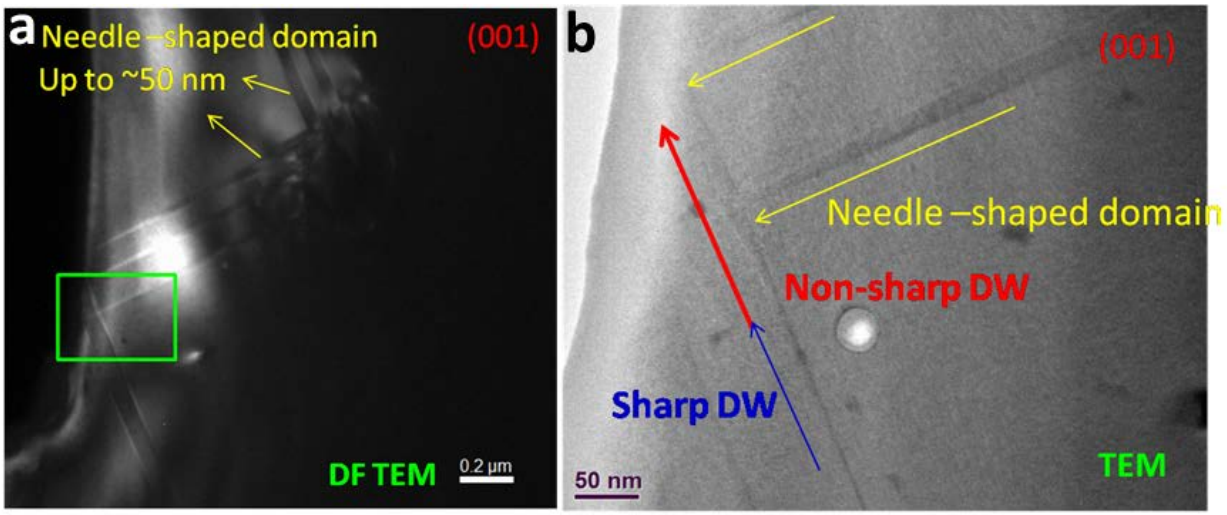

Figure S8. Domain structures of $BiVO_4$ ceramic characterized by TEM analysis. **a**, Dark field TEM image. **b**, bright field TEM image.